

Article

Magnesium Doped Hydroxyapatite-Based Coatings Obtained by Pulsed Galvanostatic Electrochemical Deposition with Adjustable Electrochemical Behavior

Diana Maria Vranceanu ¹, Ionut Cornel Ionescu ^{1,2,*}, Elena Ungureanu ¹,
Mihai Ovidiu Cojocarui ¹, Alina Vladescu ^{3,4,*} and Cosmin Mihai Cotrut ¹

- ¹ Faculty of Materials Science and Engineering, University Politehnica of Bucharest, RO060042 Bucharest, Romania; diana.vranceanu@upb.ro (D.M.V.); unguoreanu.elena14@yahoo.com (E.U.); cojocarumihaiovidui@yahoo.co.uk (M.O.C.); cosmin.cotrut@upb.ro (C.M.C.)
- ² Faculty of Dental Medicine, University of Medicine and Pharmacy “Carol Davila”, RO020021 Bucharest, Romania
- ³ Department for Advanced Surface Processing and Analysis by Vacuum Technologies, National Institute of Research and Development for Optoelectronics-INOE 2000, RO77125 Magurele, Romania
- ⁴ National Research Tomsk Polytechnic University, 634050 Tomsk, Russia
- * Correspondence: ionescu.ionut.cornel@gmail.com (I.C.I.); alinava@inoe.ro (A.V.); Tel.: +4-021-457-57-59 (A.V.)

Received: 25 June 2020; Accepted: 22 July 2020; Published: 24 July 2020



Abstract: The aim of this study was to adapt the electrochemical behavior in synthetic body fluid (SBF) of hydroxyapatite-based coatings obtained by pulsed galvanostatic electrochemical deposition through addition of Mg in different concentrations. The coatings were obtained by electrochemical deposition in a typical three electrodes electrochemical cell in galvanic pulsed mode. The electrolyte was obtained by subsequently dissolving $\text{Ca}(\text{NO}_3)_2 \cdot 4\text{H}_2\text{O}$, $\text{NH}_4\text{H}_2\text{PO}_4$, and $\text{Mg}(\text{NO}_3)_2 \cdot 6\text{H}_2\text{O}$ in ultra-pure water and the pH value was set to 5. The morphology consists of elongated and thin ribbon-like crystals for hydroxyapatite (HAp), which after the addition of Mg became a little wider. The elemental and phase composition evidenced that HAp was successfully doped with Mg through pulsed galvanostatic electrochemical deposition. The characteristics and properties of hydroxyapatite obtained electrochemically can be controlled by adding Mg in different concentrations, thus being able to obtain materials with different properties and characteristics. In addition, the addition of Mg can lead to the control of hydroxyapatite bioactive ceramics in terms of dissolution rate.

Keywords: coatings; electrochemical deposition; doped hydroxyapatite; magnesium; electrochemical behavior

1. Introduction

Intense and regular use of medical devices has resulted in hostile factors, including wearing out, micro-motions, and increase in corrosion. Thus, the challenges in the medical field are to design implantable materials with tunable properties in terms of bioactivity, biodegradation, and bactericidal effect, but the difficulties are redoubtable since these surfaces' characteristics tend to deteriorate in time.

Recently, the coatings field has attracted much interest and the ideal implant coating will likely be multifunctional, combining different technologies to promote a rapid osseointegration while inhibiting adverse tissue reactions, foreign body response or other events [1–5]. In addition to optimization of mechanical and chemical compatibilities, another important aspect for implant materials is the establishment of a suitable surface state in terms of a tailored surface topography and chemistry

that stimulates bone cell growth and activates an optimum bone osseointegration [6,7]. To achieve a successful fixation, it is important to create a stable implant-bone interface [1].

To overcome these problems, the main inorganic component in natural bone-hydroxyapatite (HAp, $\text{Ca}_{10}(\text{PO}_4)_6(\text{OH})_2$) is widely used as a bioactive coating material [8–10]. Moreover, it is possible to tailor the properties of HAp-based materials by addition of a wide variety of substitutions and ion doping found in natural bones (e.g., Mg, Zn, Sr) into its crystal structure [11–20] in search for the promotion of bone remodeling, antibacterial activity, and enhanced bio-integration. It is reasonable to deduce that by incorporation of different ions into HAp coating simultaneously could be beneficial for the improvement of both bioactivity and long-term stability such as biodegradation [21] and electrochemical behavior of the coating in physiological media [22,23].

Hydroxyapatite is a virtually ubiquitous bio-ceramic and is extensively used as a bioactive coating on Ti-based implants due to its chemical and structural similarity to hard tissues, and consequently it can be bound directly to bone. In the HAp structure, the PO_4^{3-} anions can be replaced by carbonate groups while the calcium ions by Mg^{2+} , Na^+ , K^+ , etc., and trace elements like Pb^{2+} , Cu^{2+} , and Fe^{2+} [24].

Magnesium (Mg) is also essential for metabolism, being the fourth most abundant element in the human body. Especially in the medical field, Mg has gained more and more attention from the scientific community, where it is employed either as a main or alloying element or as a substitution/doping element [25–28]. By doping HAp with Mg, the mineral metabolism can be influenced, modifying the dissolution rate of crystals and the biodegradation of the corresponding materials [29]. Landi et al. [30] showed in an *in vivo* study that Mg-HAp enhanced osseointegration and resorption, compared to commercial HAp. The substitution of Ca^{2+} by Mg^{2+} in HAp is limited due to the large size difference between Mg^{2+} and Ca^{2+} (~0.28 Å difference in radius), which leads to strong distortions of the HAp lattice, reducing its crystallinity. These changes have a direct impact on the properties of Mg-HAp, compared to their non-substituted analogues [31], by increasing their solubility. Zhao et al. reported that Mg/HAp-coated surface promotes osteogenic differentiation of pre-osteoblasts and osseointegration during the early stage of bone healing [32].

Since 1990, the interest in electrochemical deposition (ED) has evolved, getting ascendant attention as a superior method for the preparation of different protective coatings [33,34]. ED is ideal for the deposition of doped HAp coatings [13,18,35–37] due to: (i) the low temperatures involved, which enable formation of highly crystalline deposits with low solubility in body fluids and low residual stresses; (ii) the ability to coat porous and geometrically complex materials; (iii) the possible improvement of the substrate/coating bond strength; and (iv) the ability to control the thickness, composition, and microstructure of the deposit.

The aim of this study is to adapt the electrochemical behavior in synthetic body fluid (SBF) of hydroxyapatite-based coatings through addition of Mg in different concentrations obtained by pulsed galvanostatic electrochemical deposition. Magnesium was selected because it increases the solubility of HAp and thus, properties, such as the electrochemical behavior can be controlled and/or adjusted with respect to the intended medical applications. Even though indirectly, the electrochemical tests carried out in this study in synthetic body fluid (SBF) at human body temperature can be considered as a prediction tool which can indicate the potential biodegradable behavior of the proposed coatings.

2. Materials and Methods

2.1. Preparation of the Coatings

Titanium alloy (Ti6Al4V, purchased from Bibus Metals AG, Essen, Germany) discs (20 mm × 2 mm) were used as substrates. One side of each disc was metallographically prepared on silicon carbide paper of different grit (320 ÷ 800 grit). The prepared discs were cleaned with ultra-pure water, ASTM I, and iso-propyl alcohol. Before deposition, the Ti6Al4V discs were sonicated in acetone for 20 min to remove all residues and grease and cleaned with ultra-pure water.

The electrolyte used for the coating preparation is presented in Table 1 and was obtained by subsequently dissolving the chemical reagents (Table 2) in ultra-pure water. The pH was adjusted to 5 by dropwise addition of 1 M NaOH. The electrolyte was de-aerated with N₂ for 30 min to minimize the formation of CaCO₃ deposits. The temperature was maintained at 75 °C using a heating plate (KA RCT Basic Safety Control Hotplate/Stirrer and ETS-D6 Temp, IKA, Staufen, Germany) and a magnetic stirrer was used to keep the concentration of the electrolyte uniform during deposition.

Table 1. Chemical composition of the used electrolytes and sample codification.

Coating Type	Sample Codification	Chemical Composition (mM)			Molar Ratio (Ca + Mg)/P
		Ca(NO ₃) ₂ ·4H ₂ O	NH ₄ H ₂ PO ₄	Mg(NO ₃) ₂ ·6H ₂ O	
HAp	H	10.500		0	
HAp with Mg	H-Mg1	9.450	6.300	1.050	1.67
	H-Mg1.5	8.925		1.575	
	H-Mg2	8.400		2.100	

Table 2. Grade and purity of the chemical reagents employed in electrolytes preparation.

Chemical Formula	Reagent Grade	Purity	Manufacturer
Ca(NO ₃) ₂ ·4H ₂ O	ACS reagent	≥99.00%	Sigma Aldrich, Munich, Germany
NH ₄ H ₂ PO	Trace metal basis	99.99%	
Mg(NO ₃) ₂ ·6H ₂ O	ACS reagent	99.00%	
NaOH	ACS reagent	≥98.00%	

Pulsed galvanostatic deposition was carried out in a conventional three electrode electrochemical cell using a multichannel Potentiostat/Galvanostat (Parstat MC, Princeton Applied Research–Ametek, Oak Ridge, TN, USA). The deposition was performed for 40 min on Ti6Al4V discs in pulsed galvanostatic mode with a constant current density of -0.85 mA/cm^2 [12,19,38]. The activation and relaxation stages were set as follows: $i_{\text{ON}} = -0.85 \text{ mA/cm}^2$ for $t_{\text{ON}} = 1 \text{ s}$, followed by $i_{\text{OFF}} = 0 \text{ mA/cm}^2$ for $t_{\text{OFF}} = 1 \text{ s}$. After the electrochemical deposition, the samples were removed from the electrolyte and gently rinsed with ultra-pure water and stored in a desiccator. Figure 1 shows a schematic illustration of the electrochemical deposition process and the sample codification.

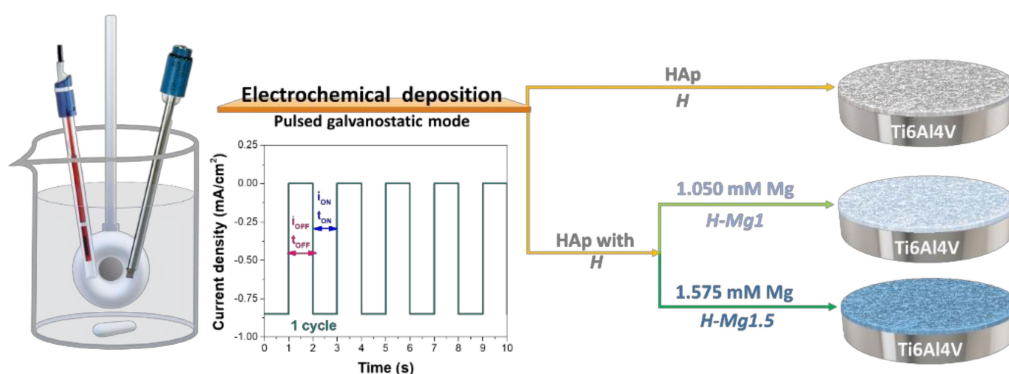


Figure 1. Schematic illustration of the electrochemical deposition process and samples codification.

As a function of Mg concentration, it was observed that up to 1.5 mM Mg(NO₃)₂·6H₂O the coatings cover the entire surface exposed to the electrochemical deposition process with a uniform and compact layer which does not present defects. By increasing the Mg concentration to 2 mM, the uniformity and compactness of the coating begins to alter indicating that an increased quantity of Mg (higher than 1.5 mM) can lead to a porous, irregular, and heterogenous coating which does not meet

the minimal criteria selection (for electrochemical investigation) and thus, this coating was not further investigated (H-Mg₂).

2.2. Characterization of Coatings

The coatings' morphology and elemental composition were investigated by scanning electron microscopy equipped with an X-ray energy dispersive spectrometer (SEM-EDS, Phenom ProX, Phenom World, Eindhoven, Netherlands).

The phase composition of the investigated samples was examined using a SmartLab X-ray diffractometer (Rigaku, city, Japan) with a CuK α radiation ($\lambda = 1.5405 \text{ \AA}$). Grazing incidence measurements were performed in the $\theta/2\theta$ range of 20–60° with a 0.02° step, at an incidence angle of 3°. For this purpose, a medium resolution parallel beam optical system was used.

Surface roughness was measured over a length of 4000 μm using DEKTAK 150 (Veeco Instruments, Plainview, NY, USA) stylus profilometer. The thickness of the coatings was determined by Dektak 150 stylus profilometer (stylus radius of 12.5 μm), measuring the forming ledge between the deposited film and the uncoated substrate.

The adhesion between the Ti6Al4V substrate and the undoped and doped HAp coatings was measured by performing a "tape test" according to ASTM D3359-17 standard [39] with an Elcometer 107 Cross Hatch Adhesion Tester kit (Ulmer, Aalen, Germany). The test consists of $6 \times 6 \text{ mm}^2$ parallel cuts with gaps of 1 mm between them made with a cutting edge that will generate a lattice pattern. It is important to apply sufficient pressure to ensure that the cutting edge will go through the coating to the substrate's surface. The adhesive tape (ISO/ASTM tape) was placed over the lattice pattern indentation, and after 90 s the tape was removed by pulling in a single smooth action at angle of 180° to the coating surface. After the adhesion tests, the coatings were examined by scanning electron microscopy (SEM Phenom Pro X, Phenom World, Eindhoven, Netherlands). The coating adhesion was assessed in terms of area removed by viewing the lattice pattern indentation and was classified in terms of percentages (from highest to weakest): 5B: 0%; 4B: $\leq 5\%$ (not large than 5%); 3B: $5\% \div 15\%$; 2B: $15\% \div 35\%$; 1B: $35\% \div 65\%$; 0B: $\geq 65\%$ (larger than 65%).

Electrochemical behavior was investigated at $37 \pm 0.5 \text{ }^\circ\text{C}$ in synthetic body fluid with a pH of 7.4 using a PARSTAT 4000 Potentiostat/Galvanostat (Princeton Applied Research, Oak Ridge, TN, USA). The chemical composition of the testing media (SBF) is presented in Table 3 and was made in accordance with the receipt proposed by Kokubo [40]. For electrochemical behavior, an area of 1 cm^2 was exposed to the electrolyte (SBF). A typical three-electrode cell with the following set-up: sample as working electrode (WE), a platinum electrode was used as a counter electrode (CE), and saturated calomel (SCE) as reference electrode (RE), was used for all electrochemical measurements. The open circuit potential (OCP) was monitored for 1 h, starting right after the sample's immersion in the electrolyte and the Tafel plots were recorded from -150 (vs. OCP) to $+150 \text{ mV}$ (vs. SCE) at a scanning rate of 1 mV/s . All measurements were achieved according to the ASTM G5-94 standard (reapproved 2011) [41]. Experiments were performed in triplicate and the obtained data are presented as mean \pm SD.

Table 3. Chemical composition and reagents grade and purity used for preparation of synthetic body fluid (SBF) media (1000 mL, pH = 7.4).

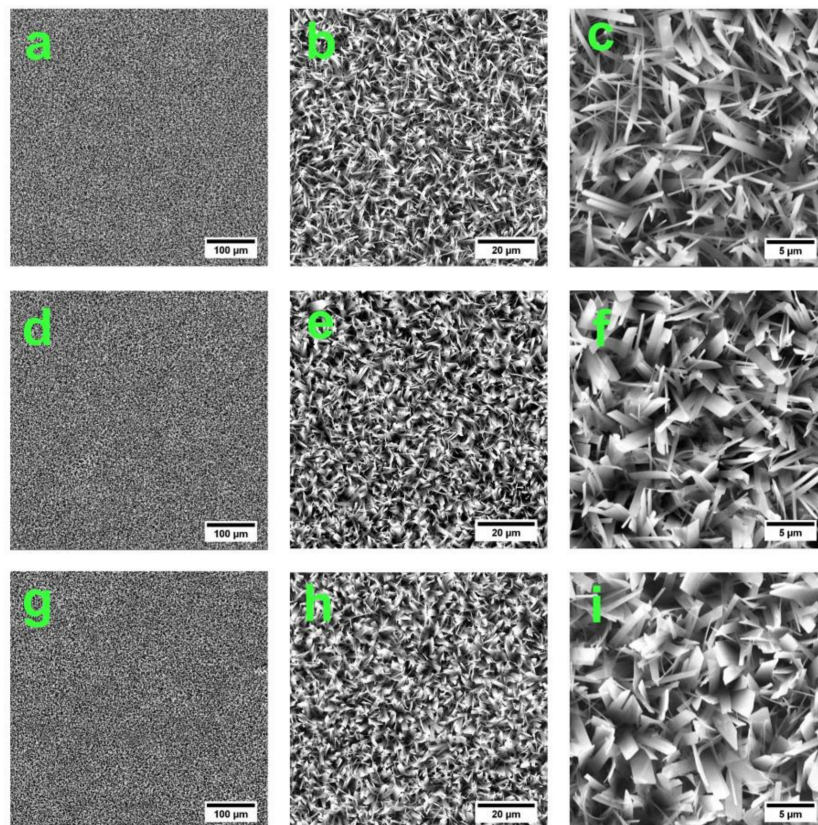
No.	Chemical Formula	Amount	Reagent Grade	Purity	Manufacturer
#1	NaCl	8.035 g/L	ACS reagent	>99.99%	Sigma Aldrich, Munich, Germany
#2	NaHCO ₃	0.355 g/L	Bio Reagent	≥99.50%	
#3	KCl	0.225 g/L	Purris p.a.	≥99.50%	
#4	K ₂ HPO ₄ ·3H ₂ O	0.231 g/L	Reagent Plus	≥99.00%	
#5	MgCl ₂ ·6H ₂ O	0.311 g/L	Purum p.a.	≥98.00%	
#6	HCl	39 mL	ACS reagent	≥37.00%	
#7	CaCl ₂	0.292 g/L	ACS reagent	≥99.00%	
#8	Na ₂ SO ₄	0.072 g/L	ACS reagent	≥99.00%	
#9	(CH ₂ OH) ₃ CNH ₂	6.118 g/L	Standard & Buffer	≥99.90%	

3. Results and Discussion

3.1. Morphology

The surface morphology and crystallinity of Hap-based coatings are in strong correlation with the current density and the electrolyte ion concentration [13,42]. Nevertheless, the cell performance and biological activity are dependent on the morphology and crystal orientation [13,43,44].

Figure 2 presents the SEM images revealing the morphology of the obtained coatings. As it can be seen, the entire investigated surface has been fully covered regardless of the electrolyte composition with a uniform layer, which also due to its morphology has a high surface to volume ratio. Particularly, for undoped HAp coatings, the morphology consists of elongated and thin ribbon-like crystals which was also reported in other studies [11,45,46].

**Figure 2.** Scanning electron microscopy (SEM) images at different magnifications evidencing the morphology of the H (a–c), H-Mg1 (d–f), and H-Mg1.5 (g–i) based coatings.

At small magnifications it was observed that, regardless of its concentration, the addition of Mg did not lead to substantial alteration of the ribbon-like morphology, while at higher magnification some dimensional variations were noted. Thus, it can be said that, compared to undoped HAp, Mg addition made the ribbons a little wider. Similar results were also found by Bakin et al. [47].

3.2. Elemental Composition

The EDS coatings analysis confirmed the presence of Mg in the H-Mg1 and H-Mg1.5 coatings and the presence of Ca and P in all coatings. The EDS mapping analysis was used to investigate elemental distribution (Ca, P, and Mg) and the results are presented in Figure 3.

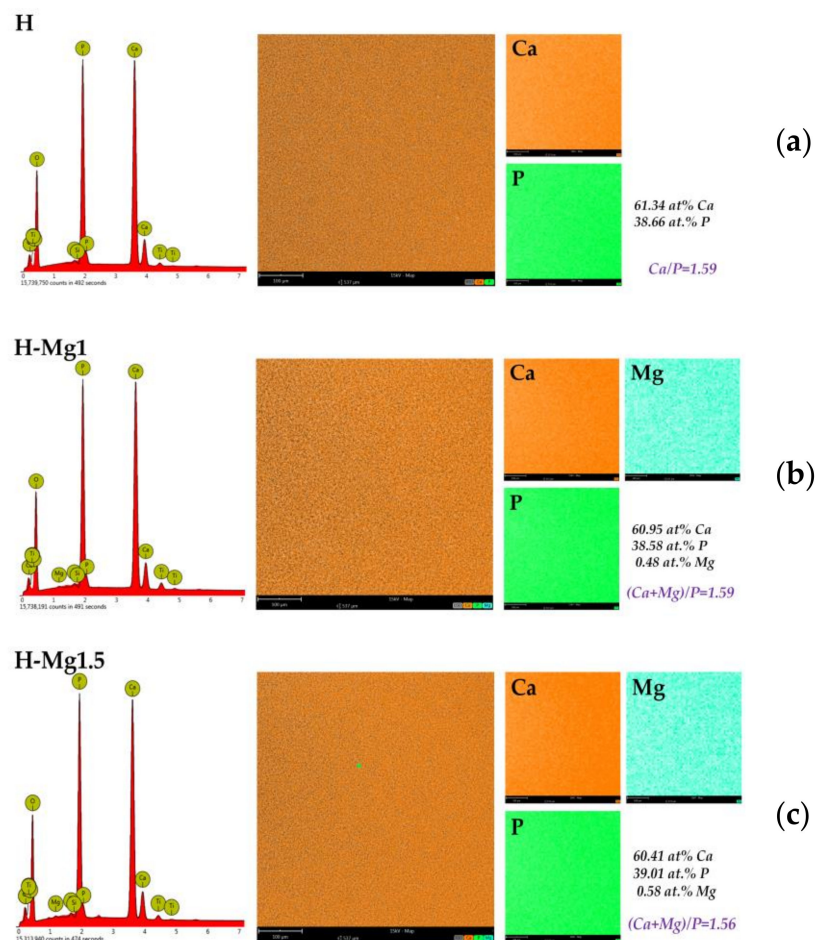


Figure 3. X-ray energy dispersive spectroscopy (EDS), elemental distribution, and chemical composition of the undoped (a) and Mg-doped hydroxyapatite (Hap) (b,c) based coatings.

According to this investigation, all elements were uniformly distributed in all three types of coatings. The $(Ca + Mg)/P$ ratio is lower than the stoichiometric one (Figure 4), suggesting that the doping process causes Ca-deficient apatite, probably due to the generation of crystal defects from the ion substitution [16]. A ratio of 1.59 was noted for H and H-Mg1 coatings, while for H-Mg1.5 the ratio was 1.56. According to some studies [48,49], Ca-deficient apatite is beneficial for bone formation, but further investigations are required.

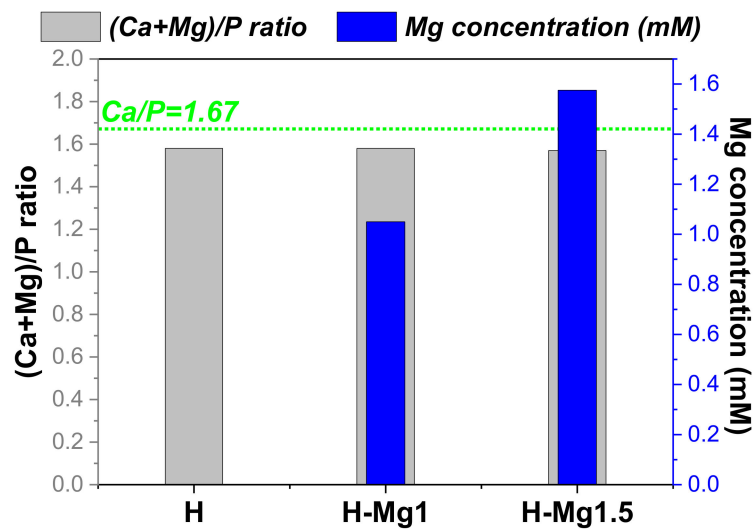


Figure 4. Dependency between (Ca+Mg)/P ratio and the Mg concentration.

3.3. Phase Composition

The X-ray diffractograms of undoped and doped HAp coatings are presented in Figure 5.

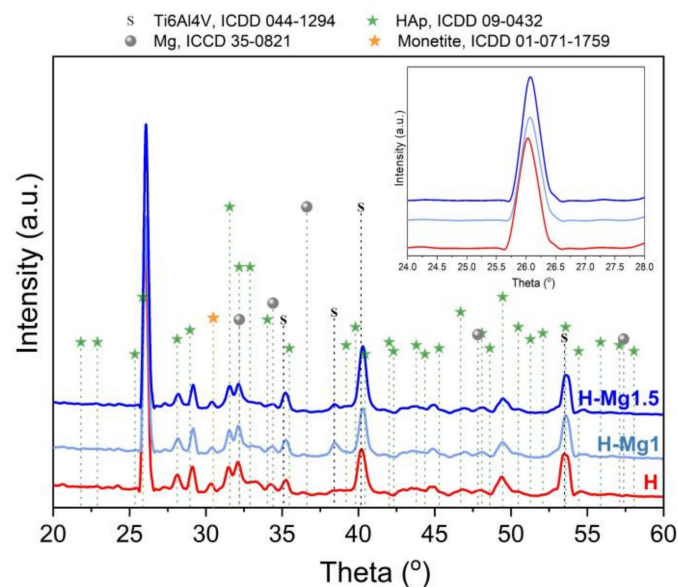


Figure 5. The X-ray diffractograms for undoped and Mg-doped HAp.

All of the coatings showed the characteristic diffraction peaks of HAp (ICDD-The International Centre for Diffraction Data, #09-0432). Nevertheless, the strongest relative intensity was registered for the plan (002) at 25.95° which is typical for electrochemical deposition [36,50,51], suggesting that the coatings are grown perpendicular on the Ti6Al4V substrate. According to the literature, oriented HAp may enable control over cells' behavior [52], and in particular the (002) preferred orientation promotes cell adhesion [53,54]. All of the coatings present a small peak which was assigned to monetite (ICDD, #01-071-1759), a precursor of hydroxyapatite. Monetite phase can be converted into hydroxyapatite by alkaline treatment [55,56]. According to the literature [57], besides its ability to regenerate bone, monetite resorbs *in vivo* faster than other calcium phosphates enabling the implant replacement by a newly formed tissue.

In the detailed diffractogram from Figure 5, it can be observed that after addition of Mg into HAp, the peak associated with (002) has slightly shifted towards higher angles from 25.95° registered for H samples to 26.06° and 26.10° for H-Mg1 and H-Mg1.5, respectively. These findings are in good correlation with other papers [19,58,59] and indicate that Mg has replaced Ca in the HAp lattice. This result is consistent with the smaller ionic radius of Mg²⁺ compared with Ca²⁺ (0.69 and 0.99 Å, respectively). No other impurities were detected.

The average crystal size was calculated using the Debye–Scherrer approximation considering the (002) peak. In the literature, it is suggested that this peak should be selected for quantitative estimations because apart from others it does not show interferences [60]. According to our results, the H coatings has a crystal size of 8.4 ± 0.1 nm, while the addition of Mg led to a slight increment of the crystal size reaching a value of 8.8 ± 0.1 and 10.2 ± 0.1 nm for H-Mg1 and H-Mg1.5, respectively; the addition of a small amount of Mg did not significantly affect the crystal size.

In the literature, there are few modalities for quantifying the degree of crystallinity. In this paper, the degree of crystallinity was calculated based on the intensity of (002) reflection peak using the equation reported in previous studies [60–62]. It was found that the crystallinity increases with respect to the Mg quantity. Thus, compared to H coatings, which presented a crystallinity of 17.8%, by increasing the Mg amount the crystallinity reaches a maximum of 29.6% for H-Mg1.5 coating, closely followed by H-Mg1 coating which had a value of 27.1%.

Based on the XRD results, it can be concluded that the hydroxyapatite-based coating become more crystalline as a function of Mg concentration. Usually, both crystallinity degree and crystal size are related with the impurity amount and the stoichiometry (Ca/P ratio). Note that for the H and H-Mg1 coatings, the Ca/P is similar, while the both H-Mg1 and H-Mg1.5 exhibited closer Mg content and probably this is the reason that the crystal size or crystallinity degree has closer values.

3.4. Roughness

The coating roughness was carried out by stylus profilometry, and the main results are presented in Table 4. As it can be seen, the average roughness and root mean square roughness parameters have increased after Mg addition, being also dependent on the quantity which has been added into the electrolyte. Figure 6 presents the representative profiles for each coating. By increasing the Mg quantity from 1 to 1.5 mM, the average roughness has increased ~8 times, passing from nanometric scale in the case of H-Mg1 to micrometric scale for the H-Mg1.5 coatings. According to the literature, the average roughness values of the commercial coated dental implants is found to be between 0.1 and 10 µm [20]. Thus, it can be noted that the developed coatings are found to be in this limitation.

The skewness parameter offers information regarding the height distribution (skew <0 for a surface with deeper valleys, skew >0 for a surface with higher peaks) [63]. Thus, it can be noted that all coatings presented positive skewness suggesting that the surface is predominantly with peaks that protrude above the mean line. By comparing the values among them, it is visible that compared to the undoped HAp, the lowest skew was registered for H-Mg1 coatings, suggesting that in this concentration, Mg reduces the peaks height and the surface tends towards a symmetrical topography, whereas increasing the Mg content leads to a very high skewness value which suggests that the surface presents very high peaks.

Table 4. Roughness parameters (Ra-average roughness, Rq-root mean square, Skew-skewness) and thickness of the investigated coatings.

Coating	Ra (nm)	Rq (nm)	Skew	Thickness (µm)
H	439.7 (±33.9)	587.9 (±66.7)	0.84 (±0.1)	11.1 (±0.9)
H-Mg1	558.2 (±37.9)	710.9 (±47.0)	0.38 (±0.1)	12.2 (±0.7)
H-Mg1.5	4396.9 (±895.4)	6609.1 (±1071.4)	2.44 (±0.25)	10.5 (±0.7)

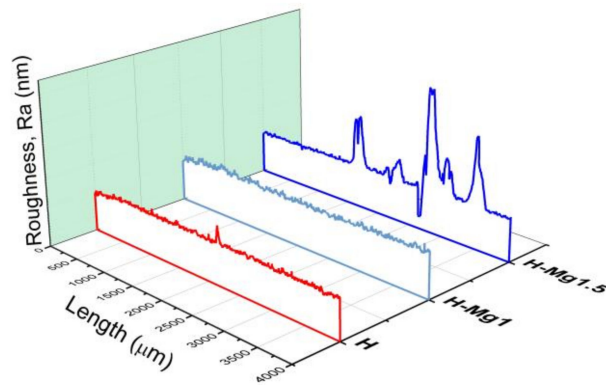


Figure 6. Representative profiles of the obtained coatings.

By measuring the forming ledge between the deposited film and the uncoated substrate, the coating thickness was obtained (Figure 7). Compared to the undoped HAp which has registered a thickness of approximately 11 μm , the H-Mg1 coatings registered an increment, until a value of $\sim 12 \mu\text{m}$, while for the H-Mg1.5, the thickness decreased, reaching the lowest thickness of 10.5 μm . The thickness differences can be associated with the deposition rate which is influenced by the Mg quantity added in the electrolyte. Considering that all the parameters involved in the electrochemical deposition were maintained constant, it can be assumed that the quantity of Mg affects the deposition rate/HAp nucleation and growth. It can be seen that for a small amount of magnesium added (1 mM), the thickness of the HAp layer increases, while after this concentration the thickness decreases. Nevertheless, Mg^{2+} ions inhibit HAp crystallization, avoiding the formation of large crystals and promoting the formation of more apatite nuclei. Thus, the presence of strong stresses inside the formed layer could be the reason why the HAp coating doped with 2.1 Mm of Mg is porous, irregular, and heterogenous. This finding can also be correlated with the fact that magnesium can inhibit apatite crystallization [64].

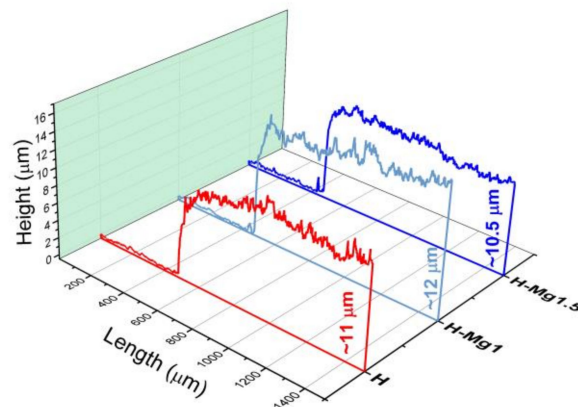


Figure 7. Coating thickness.

3.5. Adhesion

Figure 8 depicts the coatings surfaces after adhesion assays by “tape test” according to ASTM procedure. It is worth mentioning that within the adhesive tape removal, from all investigated coatings, a very thin, superficial layer was removed, without affecting the coating structural integrity, leaving behind a very consistent layer of HAp. Similar observations were also made by Parcharoen et al. [65], who investigated the adhesion between HAp-based coatings electrochemically deposited on anodized titania nanotubes of different lengths.

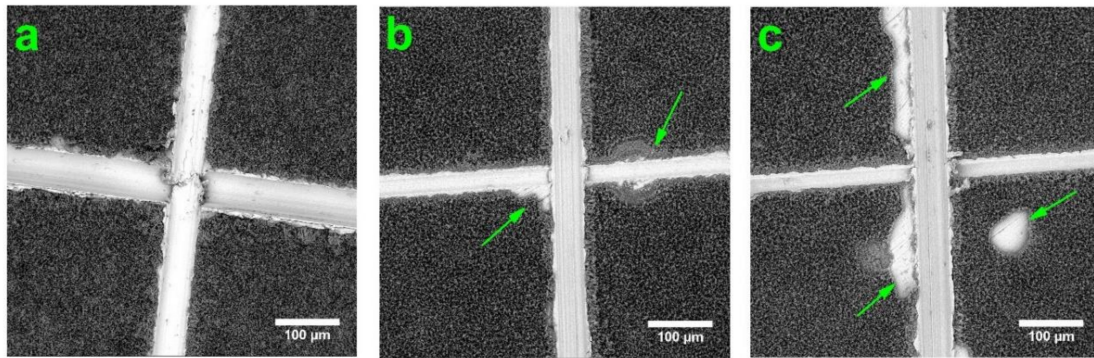


Figure 8. Representative SEM images of H (a), H-Mg1 (b), and H-Mg1.5 (c) coatings on Ti6Al4V substrate after the adhesion assay by the “tape test” (green arrow indicating the delaminated/affected areas).

Based on the obtained results after the adhesion assay, it was noted that the coatings codified with H had the best adhesion to the substrate followed closely by the coatings with 1 mM of Mg (H-Mg1). These coatings were classified according to ASTM D3359-17 [39] in the following categories: 5B for H coatings because the edges of the cuts were completely smooth with none of the lattice squares detached and 4B for H-Mg1, where some detachments/flakes, of areas not greater than 5% at the intersection of the cuts were observed. By increasing the Mg amount, it was noted that some delamination/detachment were found to be not just at the intersection of the cuts, but also along the cutting line and inside the squares of the lattice, though the affected area is not greater than 35%. Thus, the H-Mg1.5 coatings were classified into a 3B category.

Therefore, it can be concluded that even though after the adhesion assay most of the coating remained on the substrate on all of investigated samples, by increasing the Mg amount, the adhesion begins to weaken. Accordingly, the best results were obtained for H and H-Mg1 coatings, indicating that for a higher concentration of Mg (1.5 mM) the substrate may require some surface modification treatment before deposition to enhance the bonding strength at the coating–substrate interface.

3.6. Electrochemical Behaviour

Coating synthesis on titanium-based substrate enhances the biomineralization ability and acts as protection barrier against ions (especially Al and V) that can be released from the substrate improving the overall in vivo behavior and features [66]. The electrochemical techniques are a very important and useful tool in predicting a material’s behavior in vivo by analyzing the reactions at the coating–substrate interface. Figure 9 presents the open circuit potential curves and the Tafel plots of the undoped and Mg-doped coatings deposited on Ti6Al4V substrate for only one set of samples.

The polarization resistance (R_p) was calculated by using the Stern-Geary equation:

$$R_p = \frac{1}{2.3 \cdot i_{corr}} \cdot \frac{\beta_a \cdot |\beta_c|}{\beta_a + |\beta_c|} \quad (1)$$

where R_p is the polarization resistance, β_a and β_c are the anodic and cathodic Tafel slopes respectively, and i_{corr} is the corrosion current density.

Based on Tafel extrapolation the main electrochemical parameters were extracted and presented in Table 5.

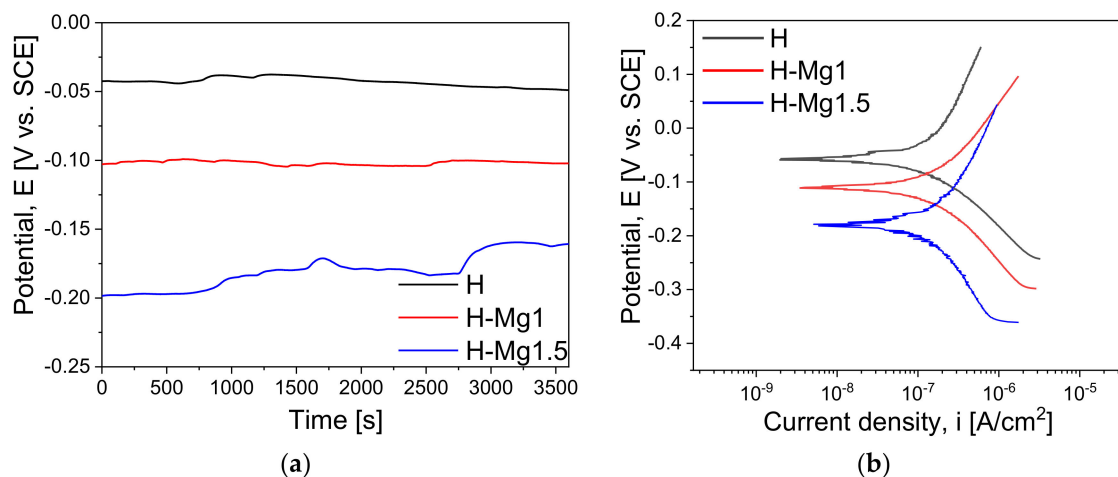


Figure 9. Open circuit potential curves (a) and Tafel plots (b) of the investigated coatings.

Table 5. Electrochemical parameters of the investigated samples (E_{oc} -open circuit potential; E_{corr} -corrosion potential; i_{corr} -corrosion current density; R_p -polarization resistance).

Sample	E_{oc} (mV)	E_{corr} (mV)	i_{corr} (nA/cm ²)	B_c (mV)	β_a (mV)	R_p (k Ω ·cm ²)
H	-48.9 (\pm 5.2)	-56.9 (\pm 6.3)	22.45 (\pm 3.82)	34.23 (\pm 5.51)	35.98 (\pm 6.15)	339.70 (\pm 10.42)
H-Mg1	-102.2 (\pm 7.8)	-110.3 (\pm 9.1)	53.70 (\pm 4.56)	63.22 (\pm 9.47)	60.67 (\pm 8.77)	250.67 (\pm 11.13)
H-Mg1.5	-160.7 (\pm 9.4)	-180.5 (\pm 10.7)	90.43 (\pm 6.75)	100.33 (\pm 12.34)	105.39 (\pm 11.92)	247.11 (\pm 12.58)

It is known that a material is resistant to the corrosive attack if it has an electropositive E_{corr} , low i_{corr} , and high R_p [67]. If we take into consideration the corrosion potential (E_{corr}), it was noted that the most electropositive value was registered for H coatings, followed by H-Mg1 and H-Mg1.5, suggesting that by increasing the Mg content the coatings' resistance to the corrosive attack of the media is poorer. Considering the corrosion current density (i_{corr}), the smallest value was registered also for H coatings, followed by H-Mg1 and H-Mg1.5 and indirectly suggesting that by adding Mg, the solubility of HAp can increase. Based on the values obtained for anodic (β_a) and cathodic (β_c) Tafel slopes of each investigated coating it can be said that the kinetics related to the electron transfer and the number and nature of electrons involved in the two reactions are also similar, indicating a mixed controlled. If we consider the obtained polarization resistance values, it was observed that the highest R_p was obtained for H followed by H-Mg1 and H-Mg1.5 coatings, suggesting the order of dissolution/biodegradability as well.

The present study highlights that the addition of Mg tailors the electrochemical behavior and so, the solubility/biodegradability of HAp. Overall, the findings are in good correlation with a study performed by Cai et al. [68], in which they found that the by increasing the Mg content a higher dissolution rate can be obtained due to the incorporation of Mg into HAp.

4. Conclusions

In this study, Mg in different concentrations was incorporated in HAp structure by electrochemical deposition method using galvanic pulses technique on Ti6Al4V substrate. All coatings presented a morphology consisting of ribbon-like crystals.

Compared with undoped HAp coatings, the ribbon-like crystals appear to increase their dimension as a function of Mg concentration added in the electrolyte. The coatings were preferentially oriented in the (002) direction which is typical for electrochemical deposition and after addition of Mg some small shift towards higher angles were noted indicating that the substitution occurred in the HAp lattice. Furthermore, Mg addition led to a higher degree of crystallinity and crystal size, compared to undoped

HAp. The (Ca + Mg)/P ratio was 1.59 for H and H-Mg1 and 1.56 for H-Mg1.5, suggesting that by increasing the Mg amount, the ratios tend towards lower values. Adhesion assays evidenced that a concentration of 1.5 mM of Mg in the electrolyte leads to a weaker adhesion, while using just 1 mM the adhesion is closer to the undoped HAp-based coatings. The electrochemical behavior highlighted that undoped HAp presented the most electropositive corrosion potential and the highest polarization resistance. By comparing the coatings with Mg addition, it was observed that the H-Mg1.5 coatings presented the highest corrosion current density and the lowest polarization resistance suggesting the weakest electrochemical behavior in SBF media. Thus, it can be observed that by doping with Mg the electrochemically deposited HAp, the electrochemical behavior can be tuned and so, the dissolution rate as well.

In conclusion, the properties and characteristics of HAp obtained by electrochemical deposition can be controlled through addition of Mg in different concentrations, thus obtaining biomaterials with tunable properties suitable for medical applications.

Author Contributions: Conceptualization and methodology, C.M.C. and D.M.V.; investigation, E.U., I.C.I., and A.V.; data analysis and interpretation, D.M.V., A.V., and C.M.C.; writing—original draft preparation, I.C.I., C.M.C., and D.M.V.; writing—review and editing, D.M.V., M.O.C., A.V., and C.M.C. All authors have read and agreed to the published version of the manuscript.

Funding: This research has been funded by the Operational Program Human Capital of the Ministry of European Funds through the Financial Agreement 51668/09.07.2019, SMIS code 124705; by grants of the Romanian Ministry of Research and Innovation, CCCDI-UEFISCDI, projects number COFUND-ERANET-RUS-PLUS-CoatDegrabac no.68/2018 as well the Core Program of 2019 (no. 18N/2019). The XRD investigations were performed using the systems modernized by the PROINSTITUTIO Project-contract No. 19PFE/17.10.2018.

Conflicts of Interest: The authors declare no conflicts of interest.

References

1. Goodman, S.B.; Yao, Z.; Keeney, M.; Yang, F. The future of biologic coatings for orthopaedic implants. *Biomaterials* **2013**, *34*, 3174–3183. [[CrossRef](#)]
2. Surmenev, R.A.; Surmeneva, M.A.; Ivanova, A.A. Significance of calcium phosphate coatings for the enhancement of new bone osteogenesis—A review. *Acta Biomater.* **2014**, *10*, 557–579. [[CrossRef](#)]
3. Raphel, J.; Holodny, M.; Goodman, S.B.; Heilshorn, S.C. Multifunctional coatings to simultaneously promote osseointegration and prevent infection of orthopaedic implants. *Biomaterials* **2016**, *84*, 301–314. [[CrossRef](#)] [[PubMed](#)]
4. Canillas, M.; Pena, P.; de Aza, A.H.; Rodríguez, M.A. Calcium phosphates for biomedical applications. *Boletín Soc. Española Cerámica Vidr.* **2017**, *56*, 91–112. [[CrossRef](#)]
5. Furko, M.; Havasi, V.; Kónya, Z.; Grünwald, A.; Detsch, R.; Boccaccini, A.R.; Balázi, C. Development and characterization of multi-element doped hydroxyapatite bioceramic coatings on metallic implants for orthopedic applications. *Bol. La Soc. Esp. Ceram. Y Vidr.* **2018**, *57*, 55–65. [[CrossRef](#)]
6. Damiani, L.; Eales, M.G.; Nobbs, A.H.; Su, B.; Tsimbouri, P.M.; Salmeron-Sanchez, M.; Dalby, M.J. Impact of surface topography and coating on osteogenesis and bacterial attachment on titanium implants. *J. Tissue Eng.* **2018**, *9*, 1–19. [[CrossRef](#)]
7. Souza, J.C.M.; Sordi, M.B.; Kanazawa, M.; Ravindran, S.; Henriques, B.; Silva, F.S.; Aparicio, C.; Cooper, L.F. Nano-scale modification of titanium implant surfaces to enhance osseointegration. *Acta Biomater.* **2019**, *94*, 112–131. [[CrossRef](#)] [[PubMed](#)]
8. Mitran, V.; Ion, R.; Miculescu, F.; Necula, M.; Mocanu, A.-C.; Stan, G.; Antoniac, I.; Cimpean, A. Osteoblast Cell Response to Naturally Derived Calcium Phosphate-Based Materials. *Materials* **2018**, *11*, 1097. [[CrossRef](#)]
9. Dascalu, C.-A.; Miculescu, F.; Mocanu, A.-C.; Constantinescu, A.E.; Butte, T.M.; Pandele, A.M.; Ciocoiu, R.-C.; Voicu, S.I.; Ciocan, L.T. Novel Synthesis of Core-Shell Biomaterials from Polymeric Filaments with a Bioceramic Coating for Biomedical Applications. *Coatings* **2020**, *10*, 283. [[CrossRef](#)]
10. Miculescu, F.; Mocanu, A.C.; Stan, G.E.; Miculescu, M.; Maidaniuc, A.; Cimpean, A.; Mitran, V.; Voicu, S.I.; Machedon-Pisu, T.; Ciocan, L.T. Influence of the modulated two-step synthesis of biogenic hydroxyapatite on biomimetic products' surface. *Appl. Surf. Sci.* **2018**, *438*, 147–157. [[CrossRef](#)]

11. Bhattacharjee, A.; Gupta, A.; Verma, M.; Anand, M.P.; Sengupta, P.; Saravanan, M.; Manna, I.; Balani, K. Antibacterial and magnetic response of site-specific cobalt incorporated hydroxyapatite. *Ceram. Int.* **2020**, *46*, 513–522. [[CrossRef](#)]
12. Thanh, T.T.; Cotrut, C.M.; Vranceanu, M.D.; Ungureanu, E.; Tarcolea, M. Studies of microstructure and composition of modified hydroxyapatite coatings via SEM investigations. *U.P.B. Sci. Bull. Ser. B* **2020**, *82*, 145–154.
13. Huang, Y.; Hao, M.; Nian, X.; Qiao, H.; Zhang, X.; Zhang, X.; Song, G.; Guo, J.; Pang, X.; Zhang, H. Strontium and copper co-substituted hydroxyapatite-based coatings with improved antibacterial activity and cytocompatibility fabricated by electrodeposition. *Ceram. Int.* **2016**, *42*, 11876–11888. [[CrossRef](#)]
14. Li, T.; Ling, L.; Lin, M.; Peng, H.; Ren, H.; Lou, C.-W.; Lin, J.-H. Recent advances in multifunctional hydroxyapatite coating by electrochemical deposition. *J. Mater. Sci.* **2020**, *55*, 6352–6374. [[CrossRef](#)]
15. Sharma, M.; Nagar, R.; Meena, V.K.; Singh, S. Electro-deposition of bactericidal and corrosion-resistant hydroxyapatite nanoslabs. *RSC Adv.* **2019**, *9*, 11170–11178. [[CrossRef](#)]
16. Munirathinam, B.; Jaladurgam, N.R.; Magesh, J.; Narayanan, R.; Mol, J.M.C.; Neelakantan, L. Improved corrosion protection of titanium implant material by crystallographic texturing of Sr doped calcium phosphate electrodeposits. *Thin Solid Films* **2019**, *675*, 115–121. [[CrossRef](#)]
17. Morejón-Alonso, L.; Mochales, C.; Nascimento, L.; Müller, W. Electrochemical deposition of Sr and Sr/Mg-co-substituted hydroxyapatite on Ti-40Nb alloy. *Mater. Lett.* **2019**, *248*, 65–68. [[CrossRef](#)]
18. Huang, Y.; Song, G.; Chang, X.; Wang, Z.; Zhang, X.; Han, S.; Su, Z.; Yang, H.; Yang, D.; Zhang, X. Nanostructured Ag+-substituted fluorhydroxyapatite-TiO₂ coatings for enhanced bactericidal effects and osteoinductivity of Ti for biomedical applications. *Int. J. Nanomed.* **2018**, *13*, 2665–2684. [[CrossRef](#)]
19. Vranceanu, D.M.; Tran, T.; Ungureanu, E.; Negoiescu, V.; Tarcolea, M.; Dinu, M.; Vladescu, A.; Zamfir, R.; Timotin, A.C.; Cotrut, C.M. Pulsed electrochemical deposition of Ag doped hydroxyapatite bioactive coatings on Ti6Al4V for medical purposes. *UPB Sci. Bull. Ser. B Chem. Mater. Sci.* **2018**, *80*, 173–184.
20. Yajing, Y.; Qiongqiong, D.; Yong, H.; Han, S.; Pang, X. Magnesium substituted hydroxyapatite coating on titanium with nanotubular TiO₂ intermediate layer via electrochemical deposition. *Appl. Surf. Sci.* **2014**, *305*, 77–85. [[CrossRef](#)]
21. Lin, W.-C.; Chuang, C.-C.; Wang, P.-T.; Tang, C.-M. A Comparative Study on the Direct and Pulsed Current Electrodeposition of Cobalt-Substituted Hydroxyapatite for Magnetic Resonance Imaging Application. *Materials* **2018**, *12*, 116. [[CrossRef](#)] [[PubMed](#)]
22. Vranceanu, D.M.; Parau, A.C.; Cotrut, C.M.; Kiss, A.E.; Constantin, L.R.; Braic, V.; Vladescu, A. In vitro evaluation of Ag doped hydroxyapatite coatings in acellular media. *Ceram. Int.* **2019**, *45*, 11050–11061. [[CrossRef](#)]
23. Vlădescu, A.; Pârâu, A.; Pană, I.; Cotruț, C.M.; Constantin, L.R.; Braic, V.; Vranceanu, D.M. In Vitro Activity Assays of Sputtered HAp Coatings with SiC Addition in Various Simulated Biological Fluids. *Coatings* **2019**, *9*, 389. [[CrossRef](#)]
24. Ergun, C.; Webster, T.J.; Bizios, R.; Doremus, R.H. Hydroxylapatite with substituted magnesium, zinc, cadmium, and yttrium. I. Structure and microstructure. *J. Biomed. Mater. Res.* **2002**, *59*, 305–311. [[CrossRef](#)]
25. Antoniac, I.; Miculescu, F.; Cotrut, C.; Ficai, A.; Rau, J.V.; Grosu, E.; Antoniac, A.; Tecu, C.; Cristescu, I. Controlling the Degradation Rate of Biodegradable Mg-Zn-Mn Alloys for Orthopedic Applications by Electrophoretic Deposition of Hydroxyapatite Coating. *Materials* **2020**, *13*, 263. [[CrossRef](#)]
26. Antoniac, I.; Popescu, D.; Zapciu, A.; Antoniac, A.; Miculescu, F.; Moldovan, H. Magnesium Filled Polylactic Acid (PLA) Material for Filament Based 3D Printing. *Materials* **2019**, *12*, 719. [[CrossRef](#)]
27. Vladescu, A.; Mihai Cotrut, C.; Ak Azem, F.; Bramowicz, M.; Pana, I.; Braic, V.; Birlik, I.; Kiss, A.; Braic, M.; Abdulgader, R.; et al. Sputtered Si and Mg doped hydroxyapatite for biomedical applications. *Biomed. Mater.* **2018**, *13*, 025011. [[CrossRef](#)]
28. Rau, J.V.; Antoniac, I.; Filipescu, M.; Cotrut, C.; Fosca, M.; Nistor, L.C.; Birjega, R.; Dinescu, M. Hydroxyapatite coatings on Mg-Ca alloy prepared by Pulsed Laser Deposition: Properties and corrosion resistance in Simulated Body Fluid. *Ceram. Int.* **2018**, *44*, 16678–16687. [[CrossRef](#)]
29. Bertinetti, L.; Drouet, C.; Combes, C.; Rey, C.; Tampieri, A.; Coluccia, S.; Martra, G. Surface characteristics of nanocrystalline apatites: Effect of Mg surface enrichment on morphology, surface hydration species, and cationic environments. *Langmuir* **2009**, *25*, 5647–5654. [[CrossRef](#)]

30. Landi, E.; Logroscino, G.; Proietti, L.; Tampieri, A.; Sandri, M.; Sprio, S. Biomimetic Mg-substituted hydroxyapatite: From synthesis to in vivo behaviour. *J. Mater. Sci. Mater. Med.* **2008**, *19*, 239–247. [[CrossRef](#)]
31. Chen, W.; Liu, Y.; Courtney, H.S.; Bettenga, M.; Agrawal, C.M.; Bumgardner, J.D.; Ong, J.L. In vitro anti-bacterial and biological properties of magnetron co-sputtered silver-containing hydroxyapatite coating. *Biomaterials* **2006**, *27*, 5512–5517. [[CrossRef](#)]
32. Zhao, S.; Jiang, Q.; Peel, S.; Wang, X.; He, F. Effects of magnesium-substituted nanohydroxyapatite coating on implant osseointegration. *Clin. Oral Implant. Res.* **2013**, *24*, 34–41. [[CrossRef](#)] [[PubMed](#)]
33. Bucur, A.I.; Linul, E.; Taranu, B.-O. Hydroxyapatite coatings on Ti substrates by simultaneous precipitation and electrodeposition. *Appl. Surf. Sci.* **2020**, *527*, 146820. [[CrossRef](#)]
34. Dorozhkin, S.V. Calcium orthophosphate deposits: Preparation, properties and biomedical applications. *Mater. Sci. Eng. C* **2015**, *55*, 272–326. [[CrossRef](#)]
35. Eliaz, N.; Sridh, T.M. Electrocrystallization of hydroxyapatite and its dependence on solution conditions. *Cryst. Growth Des.* **2008**, *8*, 3965–3977. [[CrossRef](#)]
36. Cotrut, C.M.; Vladescu, A.; Dinu, M.; Vranceanu, D.M. Influence of deposition temperature on the properties of hydroxyapatite obtained by electrochemical assisted deposition. *Ceram. Int.* **2017**, *44*, 669–677. [[CrossRef](#)]
37. Vladescu, A.; Vranceanu, D.M.; Kulesza, S.; Ivanov, A.N.; Bramowicz, M.; Fedonnikov, A.S.; Braic, M.; Norkin, I.A.; Koptuyug, A.; Kurtukova, M.O.; et al. Influence of the electrolyte's pH on the properties of electrochemically deposited hydroxyapatite coating on additively manufactured Ti64 alloy. *Sci. Rep.* **2017**, *7*. [[CrossRef](#)]
38. Oriň, R.; Oriň, A.; Kupková, M.; Hrubovčáková, M.; Škantárová, L.; Arlinghaus, H.F. Study of Electrochemical Deposition and Degradation of Hydroxyapatite Coated Iron Biomaterials. *Int. J. Electrochem. Sci.* **2015**, *10*, 659–670.
39. ASTM International. *Standard Test Methods for Rating Adhesion by Tape Test*; ASTM D3359-17; ASTM International: West Conshohocken, PA, USA, 2017; pp. 1–9.
40. Kokubo, T.; Takadama, H. How useful is SBF in predicting in vivo bone bioactivity? *Biomaterials* **2006**, *27*, 2907–2915. [[CrossRef](#)]
41. ASTM International. *Standard Reference Test Method for Making Potentiostatic and Potentiodynamic Anodic Polarization Measurements*; ASTM G5-94(2011)e1; ASTM International: West Conshohocken, PA, USA, 2011.
42. Li, T.-T.; Ling, L.; Lin, M.-C.; Jiang, Q.; Lin, Q.; Lou, C.-W.; Lin, J.-H. Effects of ultrasonic treatment and current density on the properties of hydroxyapatite coating via electrodeposition and its in vitro biomineralization behavior. *Mater. Sci. Eng. C* **2019**, *105*, 110062. [[CrossRef](#)]
43. Chakraborty, R.; Seesala, V.S.; Sengupta, S.; Dhara, S.; Saha, P.; Das, K.; Das, S. Comparison of Osteoconduction, cytocompatibility and corrosion protection performance of hydroxyapatite-calcium hydrogen phosphate composite coating synthesized in-situ through pulsed electro-deposition with varying amount of phase and crystallinity. *Surf. Interfaces* **2018**, *10*, 1–10. [[CrossRef](#)]
44. Huang, Y.; Zhou, G.; Zheng, L.; Liu, H.; Niu, X.; Fan, Y. Micro-/Nano- sized hydroxyapatite directs differentiation of rat bone marrow derived mesenchymal stem cells towards an osteoblast lineage. *Nanoscale* **2012**, *4*, 2484. [[CrossRef](#)] [[PubMed](#)]
45. Wang, H.; Eliaz, N.; Xiang, Z.; Hsu, H.P.; Spector, M.; Hobbs, L.W. Early bone apposition in vivo on plasma-sprayed and electrochemically deposited hydroxyapatite coatings on titanium alloy. *Biomaterials* **2006**, *27*, 4192–4203. [[CrossRef](#)]
46. Kanamoto, K.; Imamura, K.; Kataoka, N.; Oshitani, J.; Imanaka, H.; Nakanishi, K. Formation characteristics of calcium phosphate deposits on a metal surface by H₂O₂-electrolysis reaction under various conditions. *Colloids Surf. A Physicochem. Eng. Asp.* **2009**, *350*, 79–86. [[CrossRef](#)]
47. Bakin, B.; Koc Delice, T.; Tiric, U.; Birlik, I.; Ak Azem, F. Bioactivity and corrosion properties of magnesium-substituted CaP coatings produced via electrochemical deposition. *Surf. Coatings Technol.* **2016**, *301*, 29–35. [[CrossRef](#)]
48. Biemond, J.E.; Hannink, G.; Jurrius, A.M.G.; Verdonschot, N.; Buma, P. In Vivo Assessment of Bone Ingrowth Potential of Three-Dimensional E-Beam Produced Implant Surfaces and the Effect of Additional Treatment by Acid Etching and Hydroxyapatite Coating. *J. Biomater. Appl.* **2012**, *26*, 861–875. [[CrossRef](#)]
49. Šponer, P.; Strnadová, M.; Urban, K. In vivo behaviour of low-temperature calcium-deficient hydroxyapatite: Comparison with deproteinised bovine bone. *Int. Orthop.* **2011**, *35*, 1553–1560. [[CrossRef](#)]

50. Thanh, D.T.M.; Nam, P.T.; Phuong, N.T.; Que, L.X.; Van Anh, N.; Hoang, T.; Lam, T.D. Controlling the electrodeposition, morphology and structure of hydroxyapatite coating on 316L stainless steel. *Mater. Sci. Eng. C* **2013**, *33*, 2037–2045. [[CrossRef](#)]
51. Li, T.-T.; Ling, L.; Lin, M.-C.; Jiang, Q.; Lin, Q.; Lin, J.-H.; Lou, C.-W. Properties and Mechanism of Hydroxyapatite Coating Prepared by Electrodeposition on a Braid for Biodegradable Bone Scaffolds. *Nanomaterials* **2019**, *9*, 679. [[CrossRef](#)]
52. Dong, X.-L.; Zhou, H.-L.; Wu, T.; Wang, Q. Behavior Regulation of Adsorbed Proteins via Hydroxyapatite Surface Texture Control. *J. Phys. Chem. B* **2008**, *112*, 4751–4759. [[CrossRef](#)]
53. Liu, X.; He, D.; Zhou, Z.; Wang, G.; Wang, Z.; Wu, X.; Tan, Z. Characteristics of (002) Oriented Hydroxyapatite Coatings Deposited by Atmospheric Plasma Spraying. *Coatings* **2018**, *8*, 258. [[CrossRef](#)]
54. Kim, H.; Camata, R.P.; Lee, S.; Rohrer, G.S.; Rollett, A.D.; Hennessy, K.M.; Bellis, S.L.; Vohra, Y.K. Calcium Phosphate Bioceramics with Tailored Crystallographic Texture for Controlling Cell Adhesion. *MRS Proc.* **2006**, 925. [[CrossRef](#)]
55. Zou, Z.; Liu, X.; Chen, L.; Lin, K.; Chang, J. Dental enamel-like hydroxyapatite transformed directly from monetite. *J. Mater. Chem.* **2012**, *22*, 22637. [[CrossRef](#)]
56. Mišković-Stanković, V.B. Electrophoretic Deposition of Ceramic Coatings on Metal Surfaces. In *Electrodeposition and Surface Finishing: Fundamentals and Applications*; Stojan, S.D., Ed.; Springer: New York, NY, USA, 2014; pp. 133–216. ISBN 978-1-4939-4830-7.
57. Tamimi, F.; Le Nihouannen, D.; Eimar, H.; Sheikh, Z.; Komarova, S.; Barralet, J. The effect of autoclaving on the physical and biological properties of dicalcium phosphate dihydrate bioceramics: Brushite vs. monetite. *Acta Biomater.* **2012**, *8*, 3161–3169. [[CrossRef](#)] [[PubMed](#)]
58. Batra, U.; Kapoor, S.; Sharma, S. Influence of Magnesium Ion Substitution on Structural and Thermal Behavior of Nanodimensional Hydroxyapatite. *J. Mater. Eng. Perform.* **2013**, *22*, 1798–1806. [[CrossRef](#)]
59. Gopi, D.; Karthika, A.; Nithiya, S.; Kavitha, L. In vitro biological performance of minerals substituted hydroxyapatite coating by pulsed electrodeposition method. *Mater. Chem. Phys.* **2014**, *144*, 75–85. [[CrossRef](#)]
60. Rusu, V.M.; Ng, C.H.; Wilke, M.; Tiersch, B.; Fratzl, P.; Peter, M.G. Size-controlled hydroxyapatite nanoparticles as self-organized organic-inorganic composite materials. *Biomaterials* **2005**, *26*, 5414–5426. [[CrossRef](#)]
61. Landi, E.; Tampieri, A.; Celotti, G.; Sprio, S. Densification behaviour and mechanisms of synthetic hydroxyapatites. *J. Eur. Ceram. Soc.* **2000**, *20*, 2377–2387. [[CrossRef](#)]
62. Poralan, G.M.; Gambe, J.E.; Alcantara, E.M.; Vequizo, R.M. X-ray diffraction and infrared spectroscopy analyses on the crystallinity of engineered biological hydroxyapatite for medical application. *IOP Conf. Ser. Mater. Sci. Eng.* **2015**, *79*, 012028. [[CrossRef](#)]
63. Leach, R. Surface Topography Characterisation. In *Fundamental Principles of Engineering Nanometrology*; Elsevier: Amsterdam, The Netherlands, 2014; pp. 241–294.
64. Mayer, I.; Schlam, R.; Featherstone, J.D. Magnesium-containing carbonate apatites. *J. Inorg. Biochem.* **1997**, *66*, 1–6. [[CrossRef](#)]
65. Parcharoen, Y.; Kajitvichyanukul, P.; Sirivisoot, S.; Termsuksawad, P. Hydroxyapatite electrodeposition on anodized titanium nanotubes for orthopedic applications. *Appl. Surf. Sci.* **2014**, *311*, 54–61. [[CrossRef](#)]
66. Zhang, Z.; Dunn, M.F.; Xiao, T.D.; Tomsia, A.P.; Saiz, E. Nanostructured Hydroxyapatite Coatings for Improved Adhesion and Corrosion Resistance for Medical Implants. *MRS Proc.* **2001**, 703. [[CrossRef](#)]
67. Baboian, R.; Scully, J.R.; Dean, S.W.J. *Corrosion Tests and Standards*; Fontana, M.G., Staehle, R.W., Eds.; Springer US Plenum Press: New York, NY, USA, 2005; Volume 6, ISBN 978-1-4684-8988-0.
68. Cai, Y.; Zhang, S.; Zeng, X.; Wang, Y.; Qian, M.; Weng, W. Improvement of bioactivity with magnesium and fluorine ions incorporated hydroxyapatite coatings via sol-gel deposition on Ti6Al4V alloys. *Thin Solid Films* **2009**, *517*, 5347–5351. [[CrossRef](#)]

